IEICE TRANS. COMMUN., VOL. E75-B, NO. 6 JUNE 1992

PAPER *Special Issue on Communication Theory*

On the Computation of 16-QAM and 64-QAM Performance in Rayleigh-Fading Channels

Peter-Marc FORTUNE†, **Lajos HANZO**† *and* **Raymond STEELE**†, *Nonmembers*

SUMMARY Quadrature Amplitude Modulation (QAM) schemes are attractive in terms of bandwidth efficiency and offer a number of subchannels with different integrities via both Gaussian and Rayleigh-fading channels. Specifically, the 16-QAM phasor constellation has two, while the 64-QAM possesses three such subchannels, which become dramatically different via Rayleigh-fading channels. The analytically derived bit error rate (BER) formulae yield virtually identical curves with simulation results, exhibiting adequate BERs for the highest integrity subchannels of both 16-QAM and 64-QAM to be further reduced by forward error correction coding (FEC). However, the BERs of the lower integrity subchannels require fading compensation to reduce their values for FEC techniques to become effective. This property creates ground for a variety of carefully matched, embedded mobile transmission schemes of different complexities. The practical implementation of such an embedded scheme is demonstrated by a low-cost, low-complexity and low-consumption 50 KBd mobile video telephone scheme offering adequate speech and image quality for channel SNRs in excess of about 20 dB via Rayleigh-fading channels.

key words: *QAM theory, modulation for microcellular fading channels*

1. Introduction

Bandwidth efficient Quadrature Amplitude Modulation (QAM) schemes have been extensively deployed via transmission media, where the prevailing channel impairments are linear distortions and Additive White Gaussian Noise (AWGN). This is the case via band and power limited satellite channels or cables, for example. The theory as well as implementation of such systems is well understood and the penalty of less power efficient linear amplifiers is accepted for the benefit of high bandwidth efficiency(1).

In mobile radio and mobile satellite systems the bandwidth efficiency is at absolute premium, but at the same time they possess hostile Rayleigh-fading channels, characterised by Rayleigh envelope probability densities (PDF) and uniformly distributed random phase(2),(3). Until quite recently, however attractive in terms of bandwidth efficiency, QAM has been thought of as unsuited for mobile channels due to the high bit error rates (BER) inflicted by the violent amplitude and phase fluctuations, even if the less power efficient Class-A amplification is found acceptable.

However, recent trends in mobile radio communications resulted in the introduction of friendlier, high capacity microcellular structures with higher signal-to-noise ratios (SNR) than in conventional large-cell environments(4). Through low transmitted powers, high SNRs and moderate excess delays microcells pave the way for lightweight, possibly solar-charged, handheld portable phones of the near future.

In this friendlier propagation environment the deployment of multilevel QAM schemes with robust speech(5)–(7) and video source codecs(8) using carefully embedded forward error correction coding (FEC) rewarded us with robust mobile audio and video telephone schemes. A comparative study of various Reed-Solomon and trellis coded 16- and 64-level QAM schemes utilising a number of fading-compensation techniques was given in Ref. (9).

In this contribution we focus our attention on the theoretical aspects of using the ubiquitous maximum Euclidean distance 16- and 64-level 'square' constellations, seen in Fig. 1 and 3, respectively, via Rayleigh-fading channels. For details of their practical deployment in various speech and video schemes the interested reader is referred to Refs. (5)–(9).

2. Square Constellation 16-QAM

In the well-known 16-QAM square constellation of Fig. 1 each constellation state is represented by a four-bit symbol, constituted by the in-phase bits i_1, i_2 and quadrature bits q_1, q_2. The quaternary quadrature components I and Q are Gray-encoded by assigning the bits 01, 00, 10 and 11 to the levels $3d$, d, $-d$ and $-3d$, respectively, in a similar fashion to a Karnough-table, where the Gray coding ensures that corrupting a transmitted phasor into any of its nearest neighbours, which is the most likely error event, results in a single bit error. QAM demodulation is carried out by independently demodulating both quadrature components I and Q against their respective decision boundaries seen in Fig. 1. Closer scrutiny of this figure reveals that half of the time the bits i_1, q_1 have a noise protection distance of d from their decision boundaries, while the half of the time this distance is $3d$. As opposed to this, the bits i_2, q_2 are always at a protection distance of d from the decision boundaries and hence are more prone to errors. Due to this property, our

Manuscript received December 6, 1991.
† The authors are with Department of Electronics, University of Southampton, U.K., SO9 5NH.

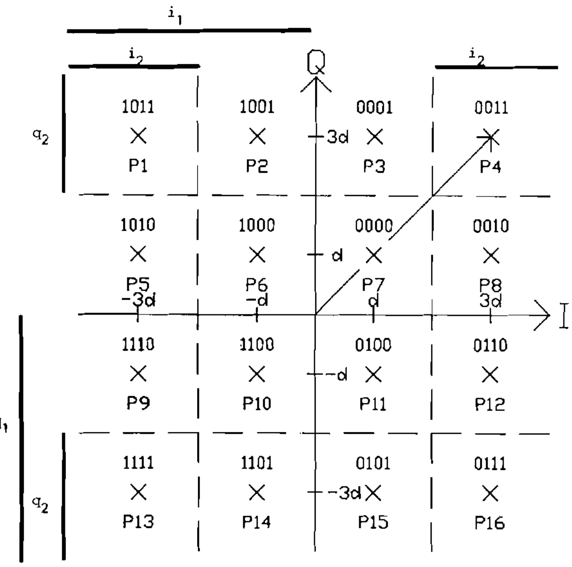

Fig. 1 16-Level QAM constellation.

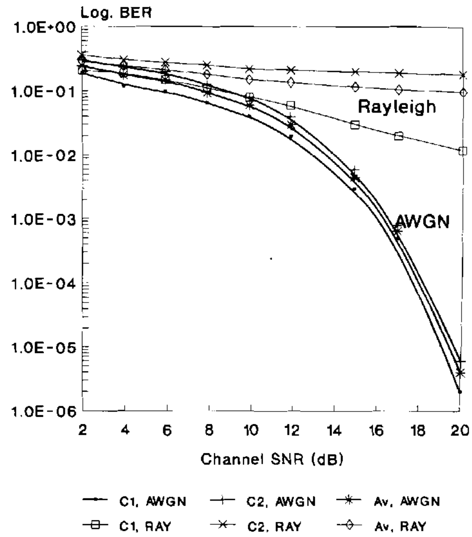

Fig. 2 C1 and C2 BER via AWGN and Rayleigh channels vs SNR.

square 16-QAM scheme can be considered, as the amalgamation of two subchannels with different integrities, which we refer to as class 1 and class 2 (C1 and C2) subchannels. The demodulation process is described as regards to the C1 subchannel in analytical terms as follows:

$$\begin{aligned} &\text{if} \quad I,\ Q \geqq 0 \quad \text{then} \quad i_1,\ q_1 = 0 \\ &\text{if} \quad I,\ Q < 0 \quad \text{then} \quad i_1,\ q_1 = 1 \end{aligned} \tag{1}$$

Taking into account the decision boundaries for the 3rd and 4th bits i_2 and q_2, respectively, as shown in Fig. 1, we have:

$$\begin{aligned} &\text{if} \quad I,\ Q \geqq 2d \quad \text{then} \quad i_2,\ q_2 = 1 \\ &\text{if} \quad -2d \leqq I,\ Q < 2d \quad \text{then} \quad i_2,\ q_2 = 0 \\ &\text{if} \quad -2d > I,\ Q \quad \text{then} \quad i_2,\ q_2 = 1. \end{aligned} \tag{2}$$

2.1 Demodulation in the Presence of AWGN

Upon demodulation in the C2 subchannel, a bit error will occur if the noise exceeds d in one direction or $3d$ in the opposite direction, where the latter probability is insignificant, and hence the C2 BER probability becomes

$$P_{2G} = Q\{d/\sqrt{N_0/2}\} = \frac{1}{\sqrt{2\pi}} \int_{d/\sqrt{N_0/2}}^{\infty} e^{(-x^2/2)} dx \tag{3}$$

where N_0 is the spectral density function of the AWGN. As the average symbol energy of the 16-level QAM constellation computed for the phasors $P_1 \cdots P_{16}$ in Fig. 1 is

$$E_0 = 10d^2, \tag{4}$$

$$P_{2G} = Q\{\sqrt{E_0/5N_0}\}. \tag{5}$$

The C1 error probability is derived by assuming equiprobable random phasors, i.e. that the bits i_1, q_1 are half of the time at a protection distance of d from the decision boundaries, and half the time the protection distance is $3d$, yielding:

$$\begin{aligned} P_{1G} &= \frac{1}{2} Q\{d/\sqrt{N_0/2}\} + \frac{1}{2} Q\{3d/\sqrt{N_0/2}\} \\ &= \frac{1}{2}[Q\{\sqrt{E_0/5N_0}\} + Q\{3\sqrt{E_0/5N_0}\}]. \end{aligned} \tag{6}$$

The C1 and C2 bit error probabilities P_{1G} and P_{2G} computed from Eqs. (5) and (6) are displayed in Fig. 2, along with the average AWGN error probability P_G, expressed as:

$$P_G = (P_{1G} + P_{2G})/2. \tag{7}$$

Our simulation results gave practically identical curves to those in Fig. 2, where the C2 subchannel shows a consistently worse performance than the C1. This performance difference becomes more pronounced via fading channels, because while the C1 performance continues to be governed by the noise due to its high average protection distance, the C2 performance suffers from the violent envelope fluctuations.

2.2 Demodulation in Rayleigh-Fading

Assuming a non-frequency-selective fading channel, where the signal bandwidth is much lower than the coherence bandwidth of the channel, the fading channel's transfer function is of the form:

$$c(t) = \alpha(t) \cdot e^{-j\Phi(t)}, \tag{8}$$

where $\alpha(t)$ represents the Rayleigh-fading envelope and $\Phi(t)$ the phase of the channel. It is general practice to assume that the phase is uniformly distributed over $[-\Pi, \Pi]$. If additionally the fading is slow, so that $\alpha(t)=\alpha$ and $\Phi(t)=\Phi$ for the duration of one signalling interval, the received signal $r(t)$ at the channel's output is:

$$r(t)=\alpha \cdot e^{-j\Phi} \cdot m(t)+n(t), \tag{9}$$

where $m(t)$ is the transmitted modulated signal and $n(t)$ is the AWGN.

On rewriting Eqs. (5) and (6) derived for the C1 and C2 subchannels as a function of E_0/N_0 in terms of the instantaneous SNR γ via Rayleigh-fading channels, we get:

$$P_{1R}(\gamma)=\frac{1}{2}[Q\{\sqrt{\gamma/5}\}+Q\{3\sqrt{\gamma/5}\}], \tag{10}$$

and

$$P_{2R}(\gamma)=Q\{\sqrt{\gamma/5}\}. \tag{11}$$

The instantaneous SNR γ fluctuates with the fading envelope, and the average BER, P_{be}, can be calculated by finding the bit error probability at a given instantaneous SNR γ and averaging it over all possible SNRs. Multiplying the bit error probability $P(\gamma)$ at the instantaneous SNR γ with the occurence probability of the specific SNR γ expressed in terms of its probability density function (PDF) $C(\gamma)$ and then integrating this product over the range of γ, we have:

$$P_{be}=\int_0^\infty P(\gamma) \cdot C(\gamma)\, d\gamma. \tag{12}$$

The random variable $\gamma=\alpha^2.E_0/N_0$ is a transformed form of the fading envelope α and the PDF of α, $C(\alpha)$ is known to be Rayleigh[(2),(3)]:

$$C(\alpha)=(\alpha/\alpha_0^2)\, e^{-\alpha^2/2\alpha_0^2}, \tag{13}$$

where α_0 is the variance of α and its second moment is given by $E(\alpha^2)=\overline{\alpha^2}=2\alpha_0^2$. As $\gamma=\alpha^2 E_0/N_0$ has two real roots, α_1 and α_2, but the Rayleigh distribution does not exist in the negative domain, α_2 can be eliminated and hence the PDF of the instanteneous SNR, $C(\gamma)$, is computed as

$$C(\gamma)=C(\alpha_1) \cdot \left|\frac{d\alpha_1}{d\gamma}\right|=\frac{1}{2\alpha_0^2}\frac{N_0}{E_0\gamma} \cdot e^{-N_0\gamma/2\alpha_0 E_0}. \tag{14}$$

We now define the average SNR Γ as:

$$\Gamma=\bar{\gamma}=E\left\{\alpha^2\frac{E_0}{N_0}\right\}=\overline{\alpha^2}\frac{E_0}{N_0}=2\alpha_0^2\frac{E_0}{N_0'} \tag{15}$$

where we exploited that $E(\alpha^2)=\overline{\alpha^2}=2\alpha_0^2$ for a Rayleigh PDF, then the transformed PDF, $C(\gamma)$, is given as below:

$$C(\gamma)=\frac{1}{\Gamma}e^{-\gamma/\Gamma}, \tag{16}$$

which is known as the Chi-square distribution[(10)], with the instantaneous SNR $\gamma \geqq 0$.

The C1 BER in Rayleigh-fading is then computed by substituting $C(\gamma)$ from Eq.(16) and $P_{1R}(\gamma)$ over Rayleigh-fading channels from Eq.(10), into Eq.(12), yielding:

$$P_{1R}(\Gamma)=\frac{1}{2\Gamma}\int_0^\infty [Q\{\sqrt{\gamma/5}\}+Q\{3\sqrt{\gamma/5}\}] \cdot e^{-\gamma/\Gamma}d\gamma. \tag{17}$$

The computation of the C2 BER is more complicated, since demodulation is now carried out on an attenuated signal constellation with the modified decision boundaries given below:

$$\begin{aligned}
&\text{if} \quad I,\ Q \geqq 2\bar{\alpha}d \quad \text{then} \quad i_2,\ q_2=1\\
&\text{if} \quad -2\bar{\alpha}d \leqq I,\ Q<2\bar{\alpha}d \quad \text{then} \quad i_2,\ q_2=0\\
&\text{if} \quad -2\bar{\alpha}d>I,\ Q \quad \text{then} \quad i_2,\ q_2=1.
\end{aligned} \tag{18}$$

Considering the case when the transmitted bit i_2 or q_2 is a logical 0 and assuming that $\alpha<2\bar{\alpha}$, the protection distance between the received phasor $\alpha \cdot d$ and the decision boundary $2\bar{\alpha}d$ becomes $d_1=(2\bar{\alpha}d-\alpha d)$. Upon substituting d_1 into Eq.(3) instead of d, we get the C2 BER for the transmission of a logical 0 as

$$P_{2,0,<2}=Q\left\{\frac{d_1}{\sqrt{N_0/2}}\right\}=Q\left\{\frac{d(2\bar{\alpha}-\alpha)}{\sqrt{N_0/2}}\right\}. \tag{19}$$

From $E_0=10d^2$, $d=\sqrt{E_0/10}$, and whence:

$$P_{2,0,<2}=Q\left\{(2\bar{\alpha}-\alpha)\sqrt{\frac{E_0}{5N_0}}\right\}. \tag{20}$$

From $\gamma=\alpha^2 E_0/N_0$ we get $E_0/N_0=\gamma/\alpha^2$, and therefore:

$$P_{2,0,<2}=Q\left\{\left(\frac{2\bar{\alpha}-\alpha}{\alpha}\right)\sqrt{\frac{\gamma}{5}}\right\}=Q\left\{\left(\frac{2\bar{\alpha}}{\alpha}-1\right)\sqrt{\frac{\gamma}{5}}\right\}. \tag{21}$$

Upon substituting Eqs.(21) and (16) into Eq.(12) we get one component of the total C2 error probability. First the upper integration boundary of Eq.(12) is derived for $\alpha \leqq 2\bar{\alpha}$ as

$$\gamma=\alpha^2 E_0/N_0 \leqq 4(\bar{\alpha})^2 E_0/N_0. \tag{22}$$

By taking into account that for a Rayleigh distribution $\bar{\alpha}=\alpha_0\sqrt{\pi/2}$:

$$\gamma=4\left(\alpha_0\sqrt{\frac{\pi}{2}}\right)^2\frac{E_0}{N_0}=2\alpha_0^2\frac{E_0}{N_0}\pi=\Gamma\pi, \tag{23}$$

and

$$P_{2,0,<2}(\Gamma)=\int_0^\infty P(\gamma)\, C(\gamma)\, d\gamma$$

$$=\int_0^{\Gamma\pi} Q\left\{\left(\frac{2\bar{a}}{a}-1\right)\sqrt{\frac{\gamma}{5}}\right\}\cdot\frac{1}{\Gamma}e^{-\gamma/\Gamma}d\gamma. \quad (24)$$

Similarly, for $d_1=(2\bar{a}d-ad)<0$, i.e., $a>2\bar{a}$, we have

$$P_{2,0,>2}=1-\left[1-Q\left\{-\frac{2\bar{a}d-ad}{\sqrt{N_0/2}}\right\}\right]$$

$$=1-Q\left\{\frac{d(2\bar{a}-a)}{\sqrt{N_0/2}}\right\}. \quad (25)$$

Exploiting $d=\sqrt{E_0/10}$ *we have*

$$P_{2,0,>2}=1-Q\left\{\sqrt{\frac{E_0}{5N_0}}(2\bar{a}-a)\right\}, \quad (26)$$

and by taking into account that $E_0/N_0=\gamma/a^2$ we arrive at:

$$P_{2,0,>2}=1-Q\left\{\left(\frac{2\bar{a}}{a}-1\right)\sqrt{\frac{\gamma}{5}}\right\}. \quad (27)$$

The lower integration limit is now identical to the previously computed upper one, i.e., $\gamma=\pi\Gamma$ and the total probability of receiving a logical one in the C2 subchannel instead of the transmitted logical zero is given by:

$$P_{2,0}(\Gamma)=P_{2,0,<2}(\Gamma)+P_{2,0,>2}(\Gamma). \quad (28)$$

Upon substituting Eqs. (16), (21) and (27) into Eq. (12), and then adding the two components according to Eq. (28) we get:

$$P_{2,0}(\Gamma)=\frac{1}{\Gamma}\int_0^{\pi\Gamma} Q\left\{\left(\frac{2\bar{a}}{a}-1\right)\sqrt{\frac{\gamma}{5}}\right\}e^{-\gamma/\Gamma}d\gamma$$
$$+\frac{1}{\Gamma}\int_{\pi\Gamma}^{\infty}\left[1-Q\left\{\left(\frac{2\bar{a}}{a}-1\right)\sqrt{\frac{\gamma}{5}}\right\}\right]e^{-\gamma/\Gamma}d\gamma. \quad (29)$$

Focusing on the opposite scenario, when a transmitted C2 logical one is corrupted into a logical zero, the modified protection distance becomes $d_1=3ad-2\bar{a}d$, which is positive, if $3ad>2\bar{a}d$, i.e., $a/\bar{a}>2/3$. The AWGN has to overcome this protection distance to cause an error, and hence the error probability for a positive protection distance d_1 is

$$P_{2,1,>2/3}=Q\left\{\left(\frac{3\bar{a}}{a}-2\right)\sqrt{\frac{\gamma}{5}}\right\}. \quad (30)$$

If the protection distance d_1 is negative, then $3ad<2\bar{a}d$, i.e., $a/\bar{a}<2/3$. In this situation the decisions are always erroneous when the noise resides above the level $-(3ad-2\bar{a}d)$, which is expressed by the aid of the Q function as:

$$P_{2,1,<2/3}=Q\left\{\frac{-(3ad-2\bar{a}d)}{\sqrt{N_0/2}}\right\}$$

$$=Q\left\{\frac{-d(3a-2\bar{a})}{\sqrt{N_0/2}}\right\}$$

or

$$P_{2,1,<2/3}=1-Q\left\{\left(\frac{3\bar{a}}{a}-2\right)\sqrt{\frac{\gamma}{5}}\right\}. \quad (31)$$

Before computing the total C2 bit error probability for the transmission of a logical one, we determine the integration limit for Eq. (12). Since $a>2\bar{a}/3$,

$$\gamma=a^2\frac{E_0}{N_0}=\left(\frac{2}{3}\bar{a}\right)^2\frac{E_0}{N_0}=\frac{4}{9}(\bar{a})^2\frac{E_0}{N_0}. \quad (32)$$

By exploiting for the Rayleigh distribution that $\bar{a}=a_0\sqrt{\pi/\gamma}$, we get:

$$\gamma=\frac{4}{9}a_0^2\frac{\pi}{\gamma}\frac{E_0}{N_0}=\Gamma\frac{\pi}{9}. \quad (33)$$

Therefore:

$$P_{2,1}(\Gamma)=P_{2,1,<2/3}(\Gamma)+P_{2,1,>2/3}(\Gamma), \quad (34)$$

or

$$P_{2,1}(\Gamma)=\frac{1}{\Gamma}\int_0^{\pi\Gamma/9} Q\left\{\left(\frac{3\bar{a}}{a}-2\right)\sqrt{\frac{\gamma}{5}}\right\}e^{-\gamma/\Gamma}d\gamma$$
$$+\frac{1}{\Gamma}\int_{\pi\Gamma/9}^{\infty}\left[1-Q\left\{\left(\frac{3\bar{a}}{a}-2\right)\sqrt{\frac{\gamma}{5}}\right\}\right]e^{-\gamma/\Gamma}d\gamma. \quad (35)$$

For random transmitted data the overall C2 subchannel error probability is given by:

$$P_{2,R}(\Gamma)=\frac{1}{2}[P_{2,1}(\Gamma)+P_{2,0}(\Gamma)]. \quad (36)$$

When we computed the C1 and C2 bit error probabilities from Eqs.(17) and (36), respectively, we received nearly identical curves to those, depicted in Fig. 2 for our simulations. Observe that the BER difference between the C1 and C2 subchannels becomes more profound than via AWGN channels and the C1 BER is sufficiently low to be further reduced by forward error correction coding (FEC), while the C2 performance requires fading-compensation to be deployed to mitigate the channel impairments[(5),(8)].

3. Square Constellation 64-QAM

In 64-level QAM (64-QAM) systems the phasors are represented by 6-bit symbols, Gray-coded to minimise the decoded error probability, as seen in Fig. 3. The 6-bit complex phasors are decomposed into the octal I and Q components. The amplitudes $7d$, $5d$, $3d$, d, $-d$, $-3d$, $-5d$ and $-7d$ of the I and Q components are assigned the 3-bit Gray codes 011, 010, 000, 001, 101, 100, 110 and 111, respectively, again, similarly to a Karnough table. Lastly, the three I and Q bits are interleaved to give a 6-bit QAM symbol represented by i_1, q_1, i_2, q_2, i_3, q_3. Similarly to 16-QAM, demodulation is carried out using the decision boundaries shown in Fig. 3 and the equations below:

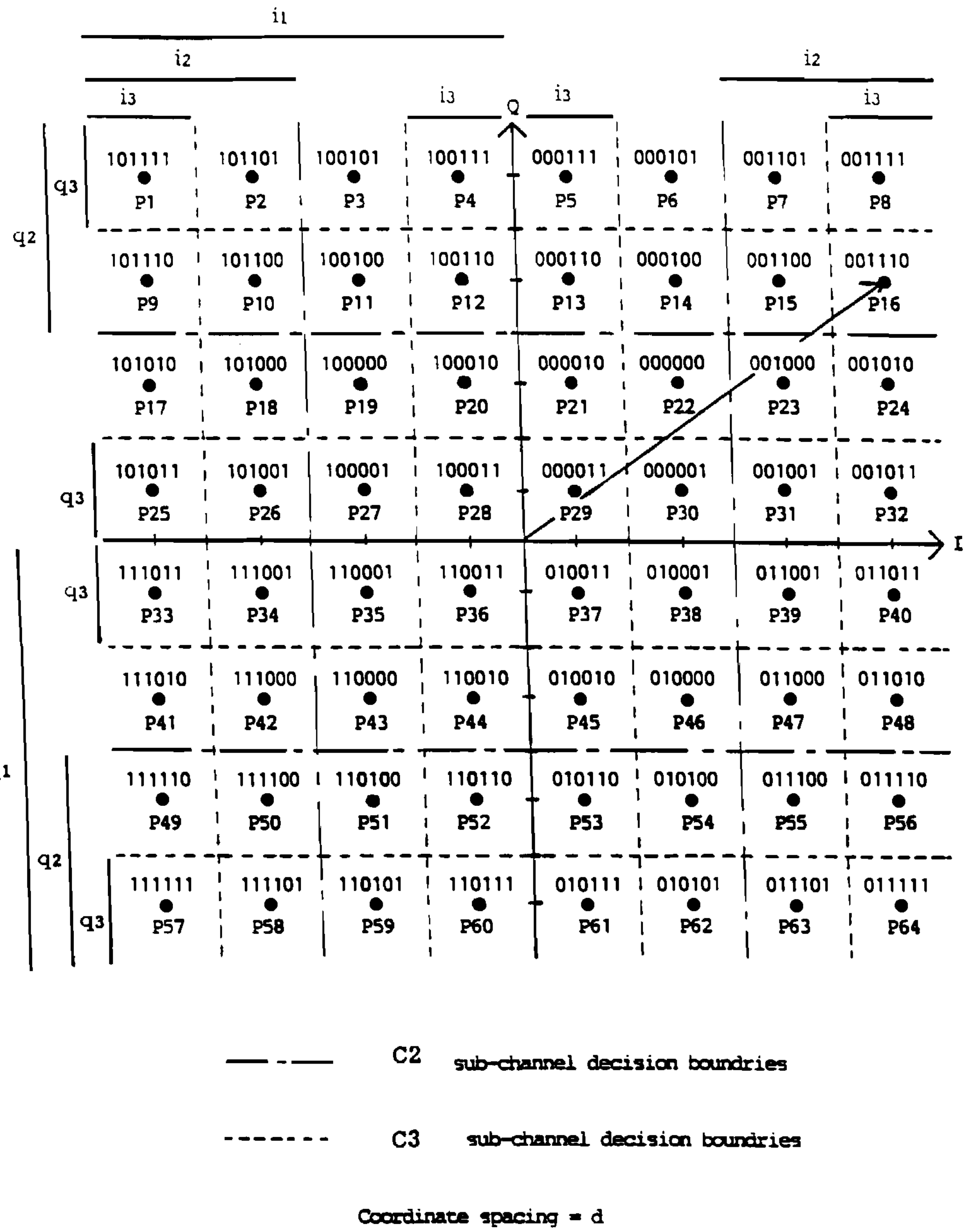

Fig. 3 64-Level QAM constellation.

$$\text{if} \quad I, Q \geqq 0 \quad \text{then} \quad i_1, q_1 = 0$$
$$\text{if} \quad I, Q < 0 \quad \text{then} \quad i_1, q_1 = 1, \qquad (37)$$

for the most significant bits, and

$$\text{if} \quad I, Q \geqq 4d \quad \text{then} \quad i_2, q_2 = 1$$
$$\text{if} \quad -4d \leqq I, Q < 4d \quad \textit{then} \quad i_2, q_2 = 0$$
$$\text{if} \quad -4d > I, Q \quad \text{then} \quad i_2, q_2 = 1, \qquad (38)$$

for the next most significant bits, and finally for the least significant bits

$$\text{if} \quad I, Q \geqq 6d \quad \text{then} \quad i_3, q_3 = 1$$
$$\text{if} \quad 2d \leqq I, Q < 6d \quad \text{then} \quad i_3, q_3 = 0$$
$$\text{if} \quad -2d \leqq I, Q < 2d \quad \text{then} \quad i_3, q_3 = 1$$
$$\text{if} \quad -6d \leqq I, Q < -2d \quad \text{then} \quad i_3, q_3 = 0$$
$$\text{if} \quad -6d > I, Q \quad \text{then} \quad i_3, q_3 = 1. \qquad (39)$$

As seen for 16-QAM before, the position of the bits in the 6-bit QAM symbol has a major effect as regards to their error probabilities. For example, the i_1, q_1 C1 bits can have a protection distance of d, $3d$, $5d$ or $7d$ from the C1 decision boundary, giving an average 'protection distance' of $16d/4=4d$. This average protection distance for the C2 i_2, q_2 bits is $2d$, while for the C3 i_3, q_3 bits it is d. Clearly, our 64-QAM modem is constituted by three subchannels of different integrities.

3.1 64-QAM Demodulation in AWGN

Assuming perfect coherent detection let us consider first the C3 subchannel's BER with its decision boundaries of $-6d$, $-2d$, $2d$ and $6d$, where each QAM symbol has a different error probability, depending on its position in the constellation of Fig. 3. For example, bit i_3 of phasor P_5, which is a logical 1, will be corrupted, if a noise sample with an amplitude in excess of d is added to it, yielding a decoding to P_6. However, when it is carried by a noise vector having larger than $5d$ amplitude over the C3 decision boundary at $6d$, the bit-decision becomes error-free again, with the erroneous decoding in P_8. In the opposite direction the decisions are error-free, until the noise amplitude reaches $-3d$, where it becomes interpreted as phasor P_3. For noise amplitudes in the range between $-3d$ and $-7d$ there are erroneous decisions, but once the $-6d$ decision boundary is exceeded, due to a negative noise sample larger than $-7d$, the received sample falls into the error-free i_3-domain again, giving the erroneous decoded phasor P_1. Based on these arguments, the i_3 bit-error probability of the P_5 phasor is given by:

$$P_{e5}=Q[d/\sqrt{N_0/2}]+Q[3d/\sqrt{N_0/2}]-Q[5d/\sqrt{N_0/2}]-Q[7d/\sqrt{N_0/2}] \quad (40)$$

with N_0 being the one-sided Gaussian noise spectral density. The average symbol energy for 64-QAM is found to be $E=42d^2$, whence substituting $d=\sqrt{E/42}$ into Eq. (40), and introducing the average SNR $\gamma=E/N_0$ gives:

$$P_{e5}=Q[\sqrt{\gamma/21}]+Q[3\sqrt{\gamma/21}]-Q[5\sqrt{\gamma/21}]-Q[7\sqrt{\gamma/21}]. \quad (41)$$

As another example, we consider phasor P_8, where the situation is entirely different, because its C3 bit i_3 is never corrupted by positive noise samples. On the other hand, for negative noise samples it cycles through erroneous and error-free zones, when the noise increases past $-d$, $-5d$, $-9d$ and $-13d$, as seen in Fig. 3, yielding an error probability of:

$$P_{e8}=Q[\sqrt{\gamma/21}]+Q[9\sqrt{\gamma/21}]-Q[5\sqrt{\gamma/21}]-Q[13\sqrt{\gamma/21}]. \quad (42)$$

Based on a similar approach, the error probabilities P_{e6} and P_{e7} are computed as follows:

$$P_{e6}=Q[\sqrt{\gamma/21}]+Q[3\sqrt{\gamma/21}]-Q[5\sqrt{\gamma/21}]+Q[9\sqrt{\gamma/21}], \quad (43)$$

$$P_{e7}=Q[\sqrt{\gamma/21}]+Q[3\sqrt{\gamma/21}]-Q[7\sqrt{\gamma/21}]+Q[11\sqrt{\gamma/21}]. \quad (44)$$

The error probabilities P_{e1}, P_{e2}, P_{e3}, P_{e4} are equivalent to those given by P_{e8}, P_{e7}, P_{e6}, P_{e5}, respectively, and the same holds for all corresponding phasors in the columns of the phasor diagram of Fig. 3. Furthermore, the q_3 bit error probability is identical to that of i_3, if independent random sequences are transmitted. Averaging the C3 bit error probabilities yields:

$$P_{C3}(\gamma)=Q[\sqrt{\gamma/21}]+\frac{3}{4}Q[3\sqrt{\gamma/21}]-\frac{3}{4}Q[5\sqrt{\gamma/21}]-\frac{1}{2}Q[7\sqrt{\gamma/21}]-\frac{1}{4}Q[9\sqrt{\gamma/21}]-\frac{1}{4}Q[11\sqrt{\gamma/21}]-\frac{1}{4}Q[13\sqrt{\gamma/21}], \quad (45)$$

where we observe that the last three terms in Eq. (45) represent extremely unlikely events as the Gaussian noise sample must exceed the $9d$ protection distance of the best protected C1 bit. Therefore these terms are neglected in our further calculations.

The C_1 and C_2 BER in AWGN is derived using our previous approach to yield:

$$P_{C2}(\gamma)=\frac{1}{2}Q[\sqrt{\gamma/21}]+\frac{1}{2}Q[\sqrt{3\gamma/21}]+\frac{1}{4}Q[\sqrt{5\gamma/21}]+\frac{1}{4}Q[\sqrt{7\gamma/21}], \quad (46)$$

and

$$P_{C1}(\gamma)=\frac{1}{4}Q[\sqrt{\gamma/21}]+\frac{1}{4}Q[\sqrt{3\gamma/21}]+\frac{1}{4}Q[\sqrt{5\gamma/21}]+\frac{1}{4}Q[\sqrt{7\gamma/21}]. \quad (47)$$

The P_{C1}, P_{C2} and P_{C3} error probability vs. channel SNR performances evaluated using Eqs. (45)-(47) are plotted in Fig. 4, which differ from our simulation results only by a fraction of a dB. In harmony with our

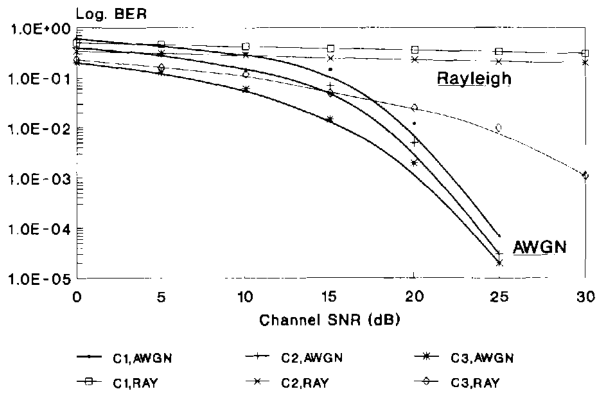

Fig. 4 C1, C2, and C3 BER via AWGN and Rayleigh channels vs. SNR.

expectations, there is consistent, but modest BER advantage when using the C1 subchannel. All subchannels have BERs$<10^{-3}$ for SNR values in excess of 23 dB and hence they are sufficiently low for speech transmission. As we will see in the next section, the higher protection distance of the C1 subchannel withstands the envelope fading and the prominance of the C1 subchannel becomes more pronounced via Rayleigh channels, as we experienced in case of 16-QAM.

3.2 64-QAM Demodulation in Rayleigh-Fading

Adopting an approach similar to that used for the 16-QAM in Sect. 2, the formula for the C1 BER via Rayleigh channels can be obtained directly by substituting the Gaussian channel result of Eq. (47) into Eq. (12) along with $C(\gamma)$ in Eq. (16), to arrive at:

$$P_{C1}(\Gamma)=\frac{1}{4\Gamma}\int_0^{\infty}\{Q[\sqrt{\gamma/21}\,]+Q[3\sqrt{\gamma/21}\,]+Q[5\sqrt{\gamma/21}\,]+Q[7\sqrt{\gamma/21}\,]\}e^{-\gamma/\Gamma}d\gamma. \tag{48}$$

Clearly, the C1 decision boundaries constituted by the coordinate axis are unaltered by the fading, but the probability of bit error for the C2 and C3 cannot be derived without considering the effects of fading on each phasor and decision boundary individually. Here we remind the reader that although the received phasors are attenuated by the instantaneous fading α, demodulation is carried out with reference to the expected value $2\alpha_0$.

Considering P_6 the modified protection distance d_1 measured from the decision boundary $4\bar{\alpha}d$ is seen from Fig. 3 to be $d_1=4\bar{\alpha}d-3\alpha d$, which, when overcome by noise, leads to erroneous decisions. If $d_1<0$, then in the absence of noise the decisions are always erroneous, while in the presence of noise the phasors can be carried back into the error-free decision zone. In both cases the error probability is given in terms of the $Q[\ \ ]$ function:

$$P_{e6}(\gamma)=Q\left[\left(\frac{4\bar{\alpha}}{\alpha}-3\right)\sqrt{\frac{\gamma}{21}}\right]. \tag{49}$$

As regards to phasor P_5 the modified protection distance from the C2 decision boundary $4\bar{\alpha}d$ is $d_1=4\bar{\alpha}d-\alpha d$, where the weight of the instantaneous attenuation α is now three times less than for P_6, giving:

$$P_{e5}(\gamma)=Q\left[\left(\frac{4\bar{\alpha}}{\alpha}-1\right)\sqrt{\frac{\gamma}{21}}\right]. \tag{50}$$

In case of P_7 the situation is considerably worse, since the modified protection distance from the C2 decision boundary at $4\bar{\alpha}d$ is seen from Fig. 3 to be $d_1=4\bar{\alpha}d-5\alpha d$, which results in:

$$P_{e7}(\gamma)=Q\left[\left(\frac{4\bar{\alpha}}{\alpha}-5\right)\sqrt{\frac{\gamma}{21}}\right]. \tag{51}$$

The most vulnerable phasor P_8 has the lowest protection distance of $d_1=4\bar{\alpha}d-7\alpha d$ and highest error probability of:

$$P_{e8}(\gamma)=Q\left[\left(\frac{4\bar{\alpha}}{\alpha}-7\right)\sqrt{\frac{\gamma}{21}}\right]. \tag{52}$$

The components of the C2 error probabilities in Eqs. (49)-(52) have to be substituted in Eq. (12) together with Eq. (16) to give the average C2 BER of:

$$\begin{aligned}P_{C2}(\Gamma)=\frac{1}{4\Gamma}\Bigg\{&\int_0^{\infty}Q\left[\left(\frac{4\bar{\alpha}}{\alpha}-1\right)\sqrt{\frac{\gamma}{21}}\right]e^{-\gamma/\Gamma}d\gamma\\&+\int_0^{\infty}Q\left[\left(\frac{4\bar{\alpha}}{\alpha}-3\right)\sqrt{\frac{\gamma}{21}}\right]e^{-\gamma/\Gamma}d\gamma\\&+\int_0^{\infty}Q\left[\left(\frac{4\bar{\alpha}}{\alpha}-5\right)\sqrt{\frac{\gamma}{21}}\right]e^{-\gamma/\Gamma}d\gamma\\&+\int_0^{\infty}Q\left[\left(\frac{4\bar{\alpha}}{\alpha}-7\right)\sqrt{\frac{\gamma}{21}}\right]e^{-\gamma/\Gamma}d\gamma\Bigg\}.\end{aligned} \tag{53}$$

The computation of the C3 subchannel performance is based on a similar approach, but for each individual phasor there are two modified protection distances, d_1 and d_2. For example, for the phasor P_6 we find $d_1=6\bar{\alpha}d-3\alpha d$ and $d_2=3\alpha d-2\bar{\alpha}d$, representing the distances from the C3 decision boundaries at $6\bar{\alpha}$d and $2\bar{\alpha}$d, respectively. Under noisy conditions the decisions are erroneous in one of two scenarios. Either, if the modified protection distance d_1 is exceeded by the noise samples, which holds for negative d_1 values as well, or if the phasor P_6 is carried across the C3 decision boundary at $2\bar{\alpha}d$ by large negative noise samples. This happens, whenever the noise value resides below the level $-d_2$. Based on these arguments, the C3 bit error probability for P_6 is computed as:

$$P_{e6}(\gamma)=Q\left[\left(\frac{6\bar{\alpha}}{\alpha}-3\right)\sqrt{\frac{\gamma}{21}}\right]+Q\left[\left(3-\frac{2\bar{\alpha}}{\alpha}\right)\sqrt{\frac{\gamma}{21}}\right]. \tag{54}$$

As regards to phasor P_5 the modified protection distances are $d_1=2\bar{\alpha}d-\alpha d$ and $d_2=6\bar{\alpha}d-\alpha d$, respectively. The decisions are erroneous, if d_1 is exceeded by noise, but noise samples larger than d_2 carry the phasors back into another error-free decision zone, leading to:

$$P_{e5}(\gamma)=Q\left[\left(\frac{2\bar{\alpha}}{\alpha}-1\right)\sqrt{\frac{\gamma}{21}}\right]-Q\left[\left(\frac{6\bar{\alpha}}{\alpha}-1\right)\sqrt{\frac{\gamma}{21}}\right]. \tag{55}$$

For phasor P_7 the modified protection distances are given by $d_1=6\bar{\alpha}d-5\alpha d$ and $d_2=5\alpha d-2\bar{\alpha}d$, yielding:

$$P_{e7}(\gamma)=Q\left[\left(\frac{6\bar{\alpha}}{\alpha}-5\right)\sqrt{\frac{\gamma}{21}}\right.$$

$$+Q\left[\left(5-\frac{2\bar{a}}{a}-1\right)\sqrt{\frac{\gamma}{21}}\right]. \quad (56)$$

Lastly, for phasor P_8 we have $d_1=7ad-6\bar{a}d$ and $d_2=7ad-2\bar{a}d$, where errors are caused by noise samples below the level $-d_1$, while for noise values below $-d_2$, the phasors are carried to another error-free zone across the decision boundary at $2\bar{a}d$, whence:

$$P_{e8}(\gamma)=Q\left[\left(7-\frac{6\bar{a}}{a}\right)\sqrt{\frac{\gamma}{21}}\right]-Q\left[\left(7-\frac{2\bar{a}}{a}\right)\sqrt{\frac{\gamma}{21}}\right]. \quad (57)$$

Assuming random input sequences and equiprobable phasors $P_1\cdots P_{64}$ we can substitute Eqs. (54)-(57), along with Eq. (16), into Eq. (12) to derive the average C3 bit error probability vs. channel SNR Γ, which is given by:

$$\begin{aligned}P_{C3}(\Gamma)=\frac{1}{4\Gamma}\Bigg\{&\int_0^\infty\left[Q\left[\left(\frac{6\bar{a}}{a}-3\right)\sqrt{\frac{\gamma}{21}}\right]\right.\\&\left.+Q\left[\left(3-\frac{2\bar{a}}{a}\right)\sqrt{\frac{\gamma}{21}}\right]\right]e^{-\gamma/\Gamma}d\gamma\\&+\int_0^\infty\left[Q\left[\left(\frac{2\bar{a}}{a}-1\right)\sqrt{\frac{\gamma}{21}}\right]\right.\\&\left.-Q\left[\left(\frac{6\bar{a}}{a}-1\right)\sqrt{\frac{\gamma}{21}}\right]\right]e^{-\gamma/\Gamma}d\gamma\\&+\int_0^\infty\left[Q\left[\left(\frac{6\bar{a}}{a}-5\right)\sqrt{\frac{\gamma}{21}}\right]\right.\\&\left.+Q\left[\left(5-\frac{2\bar{a}}{a}-1\right)\sqrt{\frac{\gamma}{21}}\right]\right]e^{-\gamma/\Gamma}d\gamma\\&+\int_0^\infty\left[Q\left[\left(7-\frac{6\bar{a}}{a}\right)\sqrt{\frac{\gamma}{21}}\right]\right.\\&\left.-Q\left[\left(7-\frac{2\bar{a}}{a}\right)\sqrt{\frac{\gamma}{21}}\right]\right]e^{-\gamma/\Gamma}d\gamma\Bigg\}. \quad (58)\end{aligned}$$

In summary, the C1, C2 and C3 subchannel performances over Rayleigh-fading channels are given by Eqs. (48), (53) and (58), respectively. The equivalent BER vs. channel SNR curves are also plotted in Fig. 4, which again coincide within a fraction of a dB with our simulation results. The BER difference between the three classes becomes more profound than via the AWGN channel portrayed in Fig. 4, as expected in harmony with our experience in case of the 16-QAM in Fig. 2. On the same note, the BER of the C1 subchannel is well suited for FEC-coded speech or image transmission, while the C2 and C3 performances have to be improved by fading-compensating automatic gain control and optional diversity reception for FEC techniques to become efficient[(6),(9)].

4. Practical QAM Mobile Systems and Conclusions

As we have seen for both 64-QAM and 16-QAM, they possess subchannels with different BERs. The subchannel integrities are consistently different via both AWGN and Rayleigh-fading channels, but their discrepancy is more dramatic via the fading channel. The subchannels with lower average protection distances have prohibitively high residual BERs, as far as their mitigation by practical FEC techniques is considered. This is because due to the received signal envelope fluctuations the multilevel QAM constellation collapses towards the origin of the coordinate system, causing excessive BERs for the low-protection subchannels. The high-protection subchannels typically withstand the channel fading better and hence their behaviour is mostly governed by the AWGN. Automatic gain control (AGC) techniques with and without channel-sounding side-information for fading compensation are reported in Refs. (5)-(9) allowing the reduced residual BERs to be cleaned up by appropriate FEC methods, rendering QAM an attractive method for bandwidth-efficient communication via mobile transmission media. In addition, the different subchannels offer a fertile ground for attractive robust and bandwidth-efficient embedded speech and video transmission schemes.

4.1 A Low-complexity Mobile Video Telephone Scheme

Based on our theoretical discourse on 16-QAM properties here we propose a practical low-cost, low-complexity and low power consumption mobile video telephone scheme for friendly microcellular channels. In this environment the SNR is sufficiently high for bandwidth-efficient 16-QAM to be deployed to moderate the excessive video bandwidth requirement of our extremely low-complexity and hence low-compression video codec. This is the pivotal point in the concept of such a system[(4)]. Then, with the proviso of the lowered signalling rate, the friendly microcellular channel becomes non-dispersive, requiring no power-hungry channel equaliser. Voice and video transmission via the C1 subchannel are feasible even without FEC coding at somewhat high channel SNR, while for the C2 subchannel FEC protection is essential[(5),(8)]. The high-compression, bandwidth-efficient voice and video codecs used in Ref. (6) and Ref. (8) have somewhat high complexities and power consumptions for our light-weight hand-held portable design, since now cost, complexity and consumption are at premium.

With the above philosophy in mind we contrived and simulated the following minimalist system, seen in Fig. 5. The CCITT 32 kbps adaptive differential pulse code modulation (ADPCM) voice codec ensures a high mean opinion score (MOS) of four at very low complexity and low bandwidth efficiency, as well as low robustness against channel errors. The low-complexity, 160 kbps, 10 frames/sec, inter-frame predictive two dimensional DPCM (2DDPCM) video

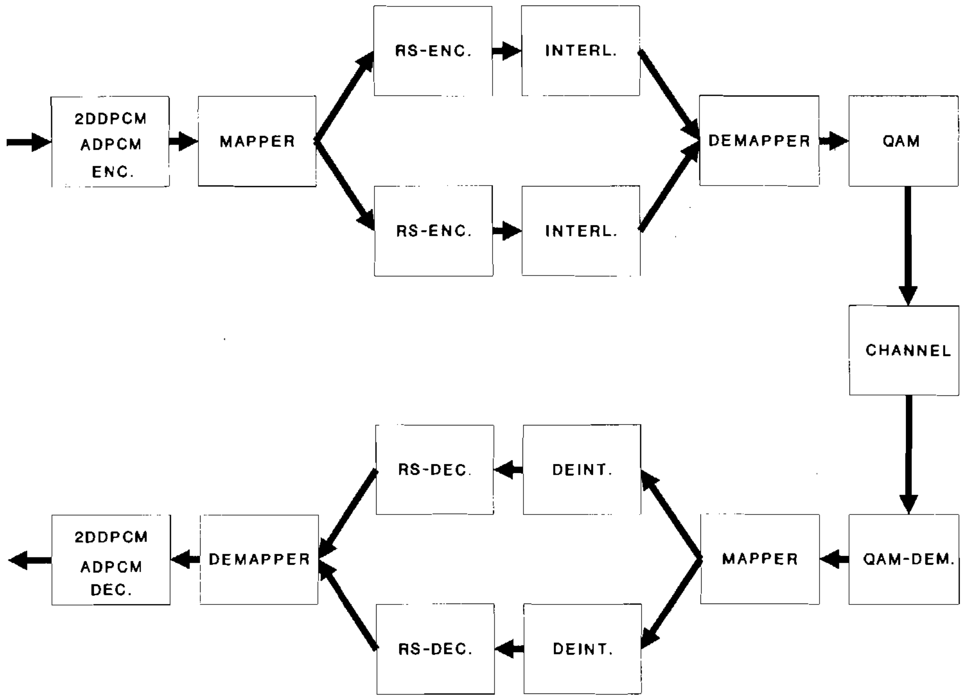

Fig. 5 System blockdiagram.

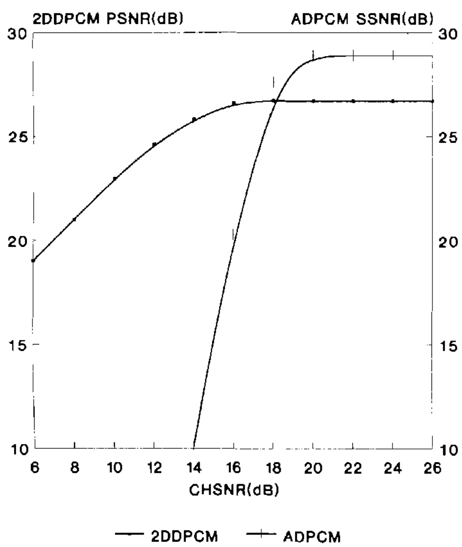

Fig. 6 2DDPCM PSNR and ADPCM SSNR with RS (12, 8, 2) coding vs. CHSNR.

codec operates on 128×128 pixels images and provides acceptable image quality for this small screen-size at high robustness against channel errors. The speech and video bits are sorted in two sensitivity classes by the 'Mapper' and FEC coded by the low-complexity RS (12, 8, 2) Reed-Solomon encoder operating over the Galois Field $GF(16)$. This encoder codes eight 4-bit symbols into 12 symbols and is capable of correcting two such symbol errors. The'Interleaver' is provided to help randomise the bursty channel errors and its output stream is directed by the 'Demapper' to the appropriate 16-QAM subchannel. The 16-QAM BER performance is improved by a fade-tracking AGC and second order diversity[(6),(8)]. The received bit-stream is then FEC-, voice-and video-decoded to reconstruct the input speech and video signals. The ADPCM speech segmental SNR (SSNR) and 2DDPCM peak SNR (PSNR) objective quality measures were evaluated for various channel SNRs in the flat Rayleigh fading channel for a pedestrian mobile speed of 3 mph and a propagation frequency of 900 MHz. Our results are seen in Fig. 6. Both the speech and video performances are virtually unimpaired for SNRs in excess of 20 dB and start to degrade below that. Observe that the adaptive DPCM speech codec rapidly collapses, when the channel injects errors, while the inherently lower quality video performance decays gracefully. The overall signalling rate is about 50 KBd, a value easily accomodated by the coherence bandwidth of typical microcellular mobile channels.

References

(1) Feher K.: "Advanced Digital Communications", Prentice-Hall (1987).

(2) Lee W. Y. C.: "Mobile Communication Engineering", McGraw-Hill (1982).

(3) Steele R.: "Mobile Radio Communications", to be published by Pentech Press, U.K. (1992).

(4) Steele R.: "The Cellular Environment of Lightweight Handheld Portables", IEEE Commun. Mag., pp. 20–29 (July 1989).

(5) Hanzo L., Steele R. and Fortune P. M.: "A Subband Coding, BCH Coding and 16-QAM System for Mobile Radio Speech Communications", IEEE Trans. Veh. Technol., **39**, 4, pp. 327-340 (Nov. 1990).
(6) Hanzo L., Salami R., Steele R. and Fortune P. M.: "Transmission of Digitally Encoded Speech at 1.2 KBd for PCN, accepted by IEE Proceedings, Part I (1991).
(7) Hanzo L., Webb W., Salami R. A. and Steele R.: "On Multilevel RPE-LTP Speech Transmission for PCN", submitted to IEE Proceedings, Part I (1991).
(8) Stedman R., Gharavi H., Hanzo L. and Steele R.: "16-QAM Transmission of Sub-band Coded Images via Microcellular Mobile Channels", submitted to IEEE Trans. Video Systems (1991).
(9) Webb W. T., Hanzo L. and Steele R.: "Bandwidth-Efficient QAM Schemes for Rayleigh-Fading Channels", IEE Proc. -I, **138**, 3, pp. 169-175 (June 1991).
(10) Proakis J. G.: "Digital Communication", McGraw-Hill (1983).

Peter-Marc Fortune received the B.Sc. and Ph.D. in electronic engineering from the University of Southampton, England in 1984 and 1988, respectively. From 1986 to 1988 he worked in communications research at the University of Southampton since which he has been studying towards the degree of Bachelor of Medicine.

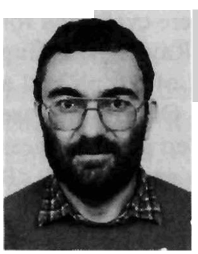

Lajos Hanzo received the M.Sc. and Ph.D. degrees in telecommunications from the Technical University of Budapest, Hungary, in 1976 and 1982, respectively. From 1976 to 1980 he was involved with research in the field of high-speed data transmission at the Telecommunications Research Institute in Budapest, Hungary, while between 1980 and 1981 he worked at the University of Erlangen-Nürnberg, West-Germany. During the years 1981-1986 his main research interest concentrated on speech communication via satellite channels. In 1986 he joined the academic staff of the University of Southampton, England, where he is involved with teaching and researching into mobile radio communications. His particular research interests cover speech and image source coding, channel coding, modulation, networking and control functions in the field of mobile radio. He authored and co-authored some sixty scientific contri-

Raymond Steele is the Managing Director of Multiple Access Communications Ltd and is Head of the Communications Research Group in the Department of Electronics and Computer Science at Southampton University. Professor Steele received a B. Sc. degree in electrical engineering from Durham University, England in 1959 and Ph.D. and D.Sc. degrees from Loughborough University of Technology, England in 1975 and 1983, respectively.Before attaining his B. Sc., Professor Steele was an indentured Apprentice Radio Engineer. After research and development posts with E. K. Cole, Cossor Radar and Electronics, and Marconi, he joined the lecturing staff at the Royal Naval College, London. He moved to Loughborough University in 1968 where he lectured and directed a research group in digital encoding of speech and picture signals. During the summers of 1975, 1977 and 1978 he was a consultant to the Acoustics Research Department at Bell Laboratories in the USA, and in 1979 he joined the company's communications Methods Research Department, Crawford Hill Laboratory, New Jersey, USA. He returned to England in 1983 to become Professor of Communications in the Department of Electronics and Computer Science at the University of Southampton, a post he retains. From 1983 to 1986 he was a non-executive director of Plessey Research and Technology and from 1983 to 1989 a consultant to British Telecom Research Laboratories. In 1986 he formed Multiple Access Communications Ltd, a company concerned with digital mobile radio systems. Professor Steele is the author of the book Delta Modulation systems (New York: Halsted, 1975) and over 150 technical publications. He is the editor of a series of books on Digital Mobile Communications, and is writing two books in the series. Professor Steele and his co-authors were awarded the Marconi Premium in 1979 and in 1989, and the Bell System Technical Journal's Best Mathematics, Communications, Techniques, Computing and Software and Social Sciences Paper in 1981. He has been a conference and session organiser of numerous international conferences and a keynote speaker at many international meetings.